Power optimization of a conical dielectric elastomer actuator for resonant robotic systems

Chongjing Cao [1 2 4 *], Xing Gao [1 3 4], Stuart Burgess [3] and Andrew T. Conn [3 4]

[1] Shenzhen Institutes of Advanced Technology, Chinese Academic of Sciences, Shenzhen, China

[2] Department of Aerospace Engineering, University of Bristol, UK

[3] Department of Mechanical Engineering, University of Bristol, UK

[4] Bristol Robotics Laboratory, Bristol, UK

* Corresponding email: cj.cao@siat.ac.cn

Abstract

Insects utilize resonant actuation to amplify the flapping stroke and improve the energy efficiency. The inherent elasticity in dielectric elastomer actuators (DEAs) offers the advantage over conventional actuators of achieving resonant actuations with no additional elastic elements required. Despite that the resonant actuation of the DEAs have attracted great research interests, no optimization has been done on the output performance of resonating DEAs. In this work, a double cone DEA (DCDEA) configuration is adopted and a numerical model is developed to characterize its dynamic response. An effective power study framework is developed and the power output of the DCDEA is optimized against its pre-stretch ratios and spacer length. To demonstrate the potential exploitation of resonant DEA performance, a bioinspired flapping wing mechanism driven by the optimized DCDEA design is developed with a peak flapping stroke of 31˚ at its resonance of 30 Hz.

Key words: dielectric elastomer actuator, power optimization, dynamic modelling, resonant actuation, flapping wing robots

1. Introduction

Bioinspired flapping wing micro air vehicles (FWMAVs) have attracted significant research interest in recent years due to the potential for highly agile flight in cluttered environments. Several FWMAV designs with the capacity of controlled flight have been developed, for example, the Microrobotic Fly [1] and DelFly [2]. One of the greatest challenges facing FWMAV designs is the extremely high power

demands required for autonomous flight at micro scales. In nature, insects minimize the power consumption by exploiting resonance. Most species utilize indirect flight muscles to deform their elastic notum, the top plate of the thorax, which elevates and depresses their wings. Their elastic thorax and muscle system form a damped oscillator and by driving this oscillator at its resonant frequency, a higher power can be exerted with an improved efficiency [3] [4].

The inherent elasticity of the emerging soft actuation technology dielectric elastomer actuators (DEAs) offer a distinguishable advantage in achieving resonant actuation over conventional actuators such as rotary motors as no additional elastic elements are required. DEAs also possess other advantages including high actuation strains, fast responses and low costs [5] [6].

The dynamic performance and the resonance of DEAs have been characterized both theoretically and experimentally using configurations such as pressurized DE balloons [7] [8], a DE minimum energy structure [9], spot DEAs [10] [11] [12], and pure shear DEAs [13] [14] [15]. The resonant actuation principle of DEAs has also been demonstrated in recent studies including vibrational crawling robots [16] [17], a rapid de-adhesion mechanism [18], a pneumatic pump [19] [20]. Insect-inspired FWMAVs have highly demanding actuation requirements in terms of the mass-specific power density [4], which makes resonant oscillation of the flapping mechanism essential. Researchers at Harvard University have demonstrated that, by using high-performing resonating DEAs, a peak mass-specific power over 600 W/kg has been achieved and tethered flight of a FWMAV driven by these artificial muscles has been reported [21]. Despite the demonstrated advantages of DEA-driven resonance in these types of robotics application with periodic excitation, to the author's knowledge, no systematic analysis has been done on characterizing and maximizing the power output performance of the DEAs at resonance.

In this work, we aim to optimize the power output of the DCDEA using the resonance principle and by tuning its design parameters (pre-stretch ratio and out-of-plane spacer length) and demonstrate the same resonant actuation principle on a flapping wing mechanism. The rest of this paper is structured as follows. In Section 2, the design and actuation principle of a DCDEA are illustrated. A dynamic model of the DCDEA is developed and verified against experiments in Section 3. Then in Section 4, optimization of the DCDEA is performed using the developed model by adjusting the pre-stretch ratio and spacer length. The optimal design is then applied to a bioinspired flapping wing mechanism design which exploits resonance and its performance is characterized in Section 5. Finally, in Section 6, the key findings are summarized and future works are discussed.

2. DCDEA design and modelling

2.1 Design overview

A schematic diagram of the DCDEA design is shown in **Figure 1** (**a**). The DCDEA consists of two membranes bonded to circular frames with an inner radius, *b*, and central disks with outer radius, *a*. The centre of the membranes are protruded by a spacer with the length, *L*. A fabricated DCDEA is shown in **Figure 1** (**b**). The actuation principle of a DCDEA is described as follows. When the DCDEA is at its passive equilibrium, the reaction forces caused by the tension on the two membranes are balanced by each other via the rigid spacer. However, when a voltage is applied across the electrodes of one DEA membrane, the generated Maxwell stress and resultant planar membrane expansion causes the spacer to move towards the actuated membrane side until another force balance is achieved [22] [23] [24] [19] (**Figure 1** (**c**)).

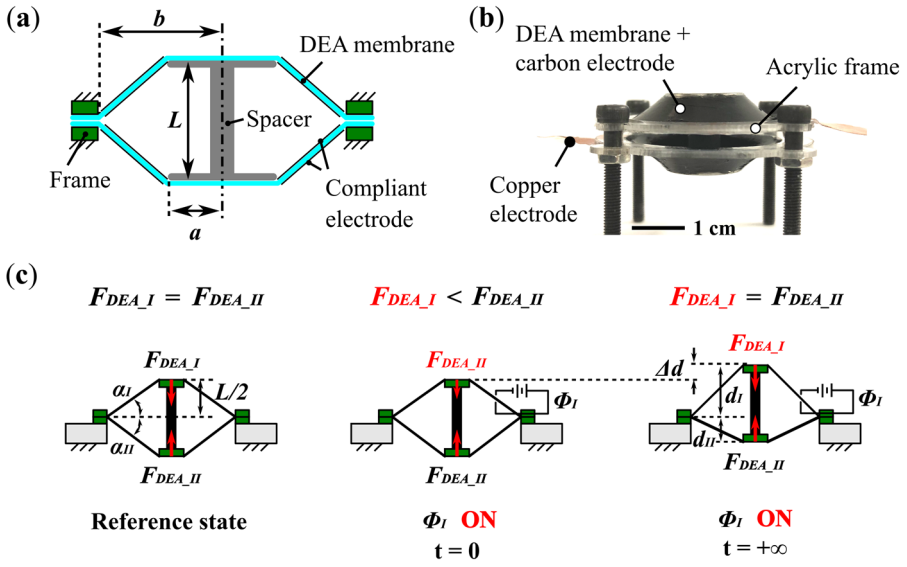

Figure 1. DCDEA design illustration. (**a**) Schematic diagram of DCDEA. (**b**) Photo of the fabricated DCDEA prototype. (**c**) Actuation principle of DCDEA. (color figure in print)

2.2 Model development

In our previous works [25] [26] [27], a dynamic model has been developed to characterize the DCDEA's dynamic electromechanical behaviour with the following assumptions made (following [28][29][30][31]): (**i**) this is a single degree-of-freedom system, i.e. only translation along the longitudinal axis is considered; (**ii**) truncated conical deformation; (**iii**) homogenous strain distribution on the membrane; (**iv**) the circumferential deformation of the membrane does not vary; (**v**) electrically, the DEA membranes are considered as an ideal capacitor with a serial resistor (i.e. assuming no leakage

current). The dynamic model is briefly described here. For detailed modelling steps please refer to our previous works [25] [26] [27].

Each piece of elastomer has the initial thickness of H_0 and is pre-stretched biaxially by $\lambda_p \times \lambda_p$ and is constrained to the support frames. The pre-stretched membranes are then deformed out-of-plane which cause an increase in the radial stretches to λ_{1_n} ($n = I, II$ for top and bottom membrane respectively) while the circumferential stretches λ_{2_n} remain constant (assumption (**iv**)). The angle between the membrane and the horizontal plane (force output angle) are α_I and α_{II}, respectively. The tension of the membranes results in forces, F_{DEA_I} and F_{DEA_II}, on the spacer along the vertical axis and the equation of motion for the spacer (neglecting gravity) can be written as

$$m\Delta\ddot{d} = -F_{DEA\_I} + F_{DEA\_II} \,, \tag{1}$$

where m is the mass of the spacer (and any payload attached), Δd is the displacement of the spacer from its passive equilibrium and F_{DEA_I} and F_{DEA_II} are the force exerted by the top and bottom membranes respectively and are expressed as

$$F_{DEA\_n} = 2\pi a H_n \, \sigma_{1\_n} \sin\alpha_n \,, \tag{2}$$

with

$$H_n = \frac{H_0}{\lambda_{1\_n}\lambda_{2\_n}} \,. \tag{3}$$

$$\lambda_{1\_I} = \frac{\sqrt{(L/2+\Delta d)^2+(b-a)^2}}{(b-a)}\lambda_p \,; \tag{4}$$

$$\lambda_{1\_II} = \frac{\sqrt{(L/2-\Delta d)^2+(b-a)^2}}{(b-a)}\lambda_p \,; \tag{5}$$

$$\sin\alpha_I = \frac{L/2+\Delta d}{\sqrt{\Delta d^2+(b-a)^2}} \,; \tag{6}$$

$$\sin\alpha_{II} = \frac{L/2-\Delta d}{\sqrt{\Delta d^2+(b-a)^2}} \,. \tag{7}$$

where σ_{1_n} ($n = I, II$) is the radial stresses of the two membranes respectively.

The Gent model [32] is adopted in this work to characterize the strain-stress relationship and the Maxwell rheological model proposed for DEAs by Foo *et al* [33] is utilized to describe the viscoelasticity of the elastomer. The Maxwell rheological model consists of two parallel branches, the first being a nonlinear spring described by the Gent model and the second being another nonlinear Gent spring in series with a dashpot. Note that only the final equations are described here, for detailed development of the Gent model based Maxwell rheological model please refer to [33].

The radial stresses are expressed as

$$\sigma_{1\_n} = \frac{\mu_1(\lambda_{1\_n}^2-\lambda_{1\_n}^{-2}\lambda_{2\_n}^{-2})}{1-(\lambda_{1\_n}^2+\lambda_{2\_n}^2+\lambda_{1\_n}^{-2}\lambda_{2\_n}^{-2}-3)/J_1} + \frac{\mu_2\left(\lambda_{1\_n}^{e\ 2}-\lambda_{1\_n}^{e\ -2}\lambda_{2\_n}^{e\ -2}\right)}{1-\left(\lambda_{1\_n}^{e\ 2}+\lambda_{2\_n}^{e\ 2}+\lambda_{1\_n}^{e\ -2}\lambda_{2\_n}^{e\ -2}-3\right)/J_2} - \varepsilon_0\varepsilon_r E_n^2 \,, \tag{8}$$

where μ_1 and μ_2 are the shear moduli of the two springs, $\lambda^e_{1\_n} = \lambda_{1\_n}/\xi_{1\_n}$ is the stretch of the spring on the second branch in the rheological model, ξ_{1_n} is the stretch of the dashpot, $\lambda^e_{2\_n} = 1$ based on assumption (**iv**), J_1 and J_2 are Gent model constants of the limiting stretches, $E_n = \Phi_{DEA\_n}/H_n$ is the electric field and Φ_{DEA_n} is the voltage across the membranes and ε_0 and ε_r are the absolute permittivity of a vacuum and the relative permittivity of the dielectric elastomer respectively.

By modelling the dashpot as a Newtonian fluid [33], the rate of deformation of the dashpot in radial axis in Eq. (8) can be described as

$$\frac{d\xi_{1\_n}}{\xi_{1\_n}dt} = \frac{1}{3\eta}\left(\frac{\mu_2\left(\lambda^{e}_{1\_n}{}^2 - \lambda^{e}_{1\_n}{}^{-2}\lambda^{e}_{2\_n}{}^{-2}\right)}{1-\left(\lambda^{e}_{1\_n}{}^2+\lambda^{e}_{2\_n}{}^2+\lambda^{e}_{1\_n}{}^{-2}\lambda^{e}_{2\_n}{}^{-2}-3\right)/J_2} - \frac{\mu_2\left(\lambda^{e}_{2\_n}{}^2 - \lambda^{e}_{1\_n}{}^{-2}\lambda^{e}_{2\_n}{}^{-2}\right)/2}{1-\left(\lambda^{e}_{1\_n}{}^2+\lambda^{e}_{2\_n}{}^2+\lambda^{e}_{1\_n}{}^{-2}\lambda^{e}_{2\_n}{}^{-2}-3\right)/J_2}\right), \quad (9)$$

where η is the coefficient of viscosity of the dashpot.

When a voltage Φ_{in_n} is applied, charge flows into the DEA membrane, and the rate of charge and voltage across the DEA membrane can be expressed as

$$\dot{Q}_n = -\frac{1}{R_s C_n} Q_n + \frac{1}{R_s}\Phi_{in\_n}\,, \quad (10)$$

$$\Phi_{DEA\_n} = \frac{1}{C_n} Q_n\,, \quad (11)$$

where Q_n is the charge accumulated on the electrodes, C_n is the capacitance of each DEA membrane and R_s is the surface resistance and is assumed to be constant in this model (following [29]).

The capacitance of each membrane can be expressed as

$$C_n = \varepsilon_0 \varepsilon_r \frac{\pi\left(b^2 - a^2\right)}{H_n \cos\alpha_n}\,. \quad (12)$$

To summarize this electromechanical model, with the input voltages, Φ_{in_n}, pre-defined, and the initial conditions known (deformations, Δd, charges in the membranes, Q_n, radial stretches of the dashpots, ξ_{1_n}), the state of the DEA at the next time step can be estimated by solving a set of ordinary differential equations (ODEs) (Eqs. 1, 9, 10) using an ODE solver in MATLAB (MathWorks).

3. Model validation

3.1 DCDEA fabrication

The DCDEA prototypes were fabricated with 100 μm thick off-the-shelf silicone elastomer (ELASTOSIL, Wacker Chemie AG) and the geometrical parameters were a = 7.5 mm, b = 15 mm, L = 7 mm. Three sets of specimens with the pre-stretch ratios of 1×1, 1.2×1.2 and 1.4×1.4 were prepared. The detailed fabrication process can be found in the supplementary material.

3.2 Quasi-static characterization

Figure 2 (**a-c**) shows the experimental setup, measured and modelled results of the quasi-static force-displacement of a single DEA membrane respectively. The experimental setup follows the previous studies [19] [25] where the DEA membrane was deformed out-of-plane at a low velocity of 0.05 mm/s to minimize the effect of viscoelasticity. Electric fields with the values of 0 and 50 V/μm were tested. Note that the model prediction agrees well with the experimental results. The Gent model parameters were determined by a least-mean-squares algorithm in MATLAB with the values of $\mu_1 = 415.5\times10^3$ Pa, $J_1 = 16$. A dielectric constant of $\varepsilon_r = 2.8$ was adopted as reported by the manufacturer.

3.3 Dynamic characterization

Frequency sweep tests from 1 to 100 Hz with a square voltage waveform were used to investigate the dynamic response of the DCDEAs and the experimental setup is shown in **Figure 2** (**d**) with detailed description available in supplementary material. Experimental and modelled results of the dynamic response of the DCDEAs with different pre-stretch ratios are shown in **Figure 2** (**e-f**) respectively. The identified viscoelasticity parameters are: $\mu_2 = 90\times10^3$ Pa, $J_2 = 20$, $\eta = 117$ Pa.s and the surface resistance R_s is estimated at 2 MΩ. Excellent accuracy was found between the modelled and measured dynamic response with all three sets of pre-stretch ratios, demonstrating the validity of this numerical model. The dynamic motion of the DCDEA at its resonance was recorded by a high-speed camera at 5000 frames-per-second (SA1.1, Photron), and its motion in one cycle is shown in **Figure 2** (**g**). Note that the amplitude at resonance can be over 20 times higher than non-resonance, and the total stroke can pass 100 % relative to its spacer length (second and fourth plot in **Figure 2** (**g**)). For the DCDEA with $\lambda_p = 1\times1$, a resonant stroke of 257 % was measured, which, to the authors' knowledge, is the highest linear stroke reported in DCDEAs to date.

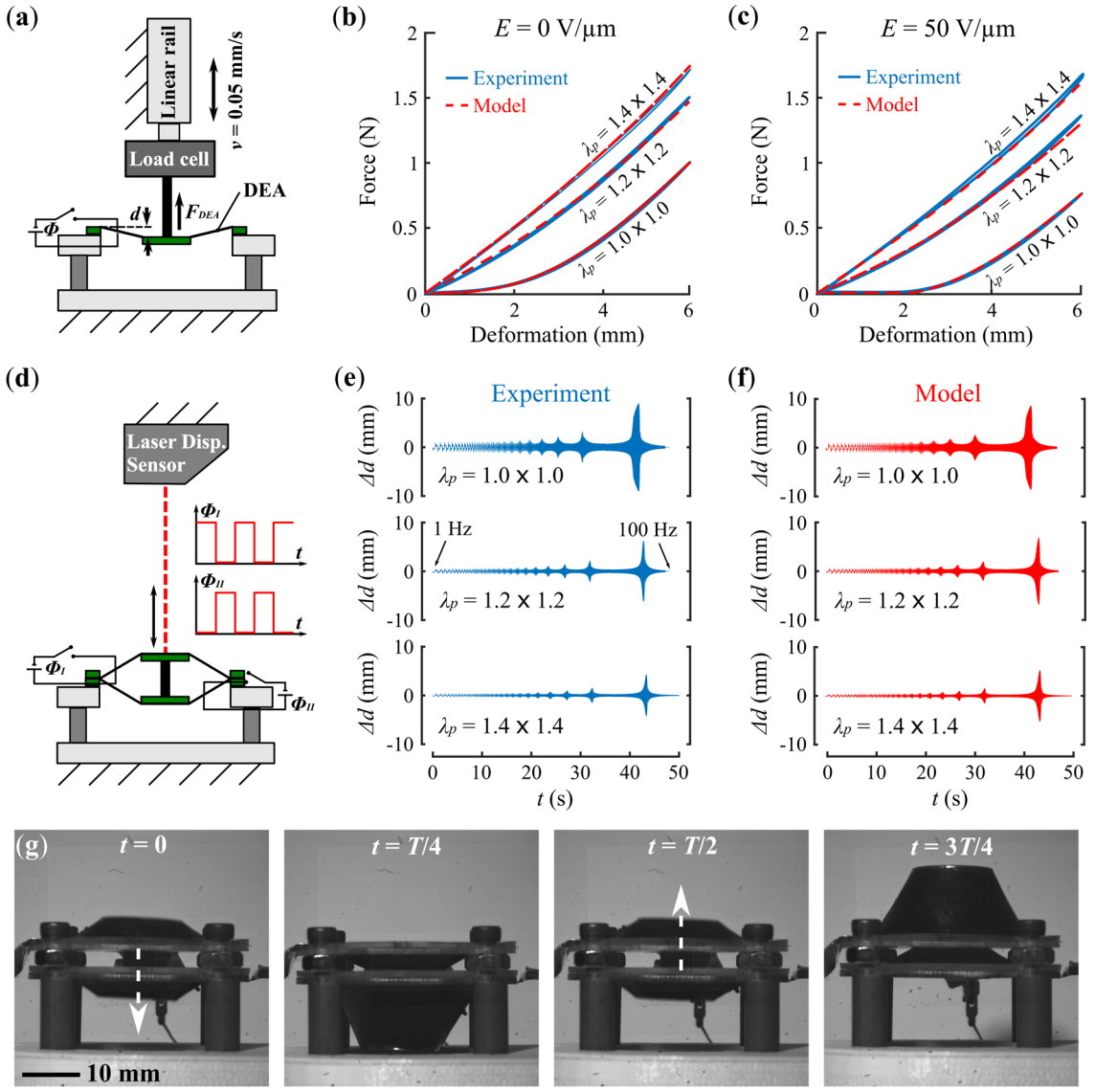

Figure 2. DCDEA model validation. (**a**) Experimental setup of quasi-static force-displacement measurement of a single cone DEA membrane. (**b-c**) Comparison of measured and modelled force-displacement relationship of the single cone DEA with different pre-stretch ratios when (**b**) $E = 0$ and (**c**) $E = 50$ V/μm. (**d**) Experimental setup of free oscillation of the DCDEA. (**e-f**) Measured and modelled dynamic response of DCDEAs with different pre-stretch ratios. (**g**) Series of photos of a DCDEA oscillating at its resonance. (multimedia file available in supplementary material) (color figure in print)

4. Power output optimization

4.1 Study setup

In this section, a modelling framework for characterizing and optimizing the power output of DEAs when driving dissipative loads is proposed by using the verified DCDEA model. The power study setup

is illustrated in **Figure 3** (**a**). A payload with a mass, *M*, and a dashpot, *c*, are rigidly attached to the DCDEA. The payload is constrained to allow horizontal translations. The equation of motion of the moving payload can be written as

$$M\Delta\ddot{d} + cv = F_{DEA}\,, \tag{13}$$

where $\Delta\ddot{d}$ and *v* are the acceleration and velocity of the mass respectively, F_{DEA} is the net force of the two membranes computed from Eq. (2).

The geometrical parameters of the DCDEA, *a* and *b*, are fixed at 7.5 mm and 15 mm respectively with the spacer length, *L*, varying from 5 to 30 mm and pre-stretch ratio varying from 1.0 to 1.4. The spacer is assumed to have a mass of 1 g and the payload has a mass of 2 g and a damping coefficient of 1 N.s/m. Two antiphase alternating current voltages are applied to the two membranes, and the frequency of the actuation voltages are stepped from 20 to 200 Hz with an increment of 0.2 Hz and 10 cycles are repeated at each frequency to ensure a steady-state response. The average power output of the DCDEA per cycle is $P_{out} = \frac{1}{T}\int_0^T cv^2\,dt$, where *T* is the period.

Increasing the voltage amplitude can improve the output of a DEA, however, breakdown can happen when the corresponding electric field passes the threshold E_b. Hence, the amplitude of the voltage in this study is determined based on the breakdown electric field and the nominal thickness of the membrane. The breakdown electric field of the ELASTOSIL silicone elastomer was shown in [34] [35] [36] as a function of two principle stretches and increases with the increasing stretch ratios. An empirical scale law was proposed in [34] based on the experimental measurements and is written as $E_b = E_{b0}\lambda_p^{1.23}$. However, it is noteworthy that all existing measurements were based on equal biaxial stretches. To cope with the different principle stretches in cone DEAs, the breakdown electric field is proposed as a product of both λ_1 and λ_2, and is written as $E_b = E_{b0}(\lambda_1\lambda_2)^{0.615}$, where E_{b0} = 80 V/μm is the breakdown electric field with no pre-stretch and as reported by the manufacturer (Wacker Chemie AG). Note that the E_{b0} adopted in this study is relatively conservative as a higher value of E_{b0} = 90 V/μm was reported in [36]. The voltage amplitude is $\Phi_{peak} = 0.8E_bH$, where a safety margin of 20% is considered when determining the voltage amplitude to further minimize the failure rate.

Figure 3 (**b**) shows the power optimization strategy and is summarized as follows. Two parameters: λ_p and *L* are varied while the others are kept constant. By using the geometrical relationship (Eq. (3-7)), the two principle stretches, membrane thickness and force output angle are obtained. Based on the breakdown strength scale law, E_b and Φ_{peak} are determined. The average power output of the DCDEA at different frequencies can be estimated by the dynamic model of DCDEA (Eq. (1,2,8-12)). Finally, the optimal λ_p and *L* values can be determined.

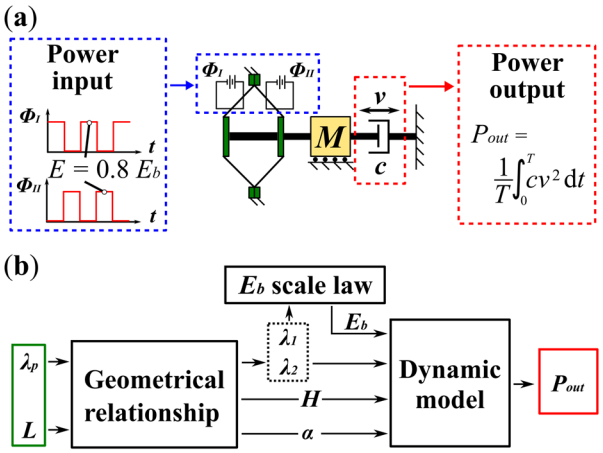

Figure 3. DCDEAs power optimization concept. (**a**) Setup for the power output optimization study. (**b**) Illustration of the power optimization strategy. (color figure in print)

4.2 Study results

Effects of pre-stretch ratios. The power output of the DCDEA with different λ_p and L values are shown in **Figure 4** with each subplot showing P_{out} as a function of excitation frequency, f, and L with λ_p fixed. For any sets of (λ_p, L), P_{out} increases with the increasing f, reaches a peak value, P_{peak}, then decreases as f increases further. The peak power output demonstrates the advantages of resonant actuation of the inherent elastic DEAs. By comparing the subplots with different pre-stretch ratios, the maximum power output, P_{max}, the DCDEA can generate reduces with the increasing λ_p. For example, P_{max} is 73.6 mW when λ_p = 1×1 and drops to 58.3 mW when λ_p becomes 1.4×1.4. This suggests that the DCDEA could have an optimal performance with no additional pre-stretch and the stretch caused by the spacer protrusion can be sufficient. This finding echoes our previous quasi-static work output optimization study on cone DEAs [37]. For the DCDEA prototype which weights ~ 1.6 g, the peak mass-specific power density is estimated at ~ 46 W/kg, which is comparable with insect muscles [38] [39].

Effects of spacer lengths. The peak power output, P_{peak}, the corresponding frequency where the peak power occurs, f_{peak}, and the peak stroke, Δd_{peak}, for DCDEAs with λ_p = 1×1 and varying L are plotted in **Figure 5** (**a**). P_{peak} shows an increase with the increasing L and peaks at 21 mm, then drops while Δd_{peak} fluctuates and shows a peak at L = 19 mm. f_{peak} demonstrates a continuous increase with the L value. The different L values where power and stroke peaks at suggests DCDEA design should be tailored based on the desired output (i.e. stroke or power). The correlation between the spacer length and the output of the DCDEA can be explained by that the output angle α increases as L increases, hence the force F_{DEA} (Eq. (2)), which increases the DCDEA performance. However, if the spacer becomes too long, the radial stretch on the membranes can be extremely high, which causes the strain stiffing (Eq. (8)) and reduces the performance. For all five cases with different pre-stretch ratios, a medium L value between 13 to 21 mm ($41^\circ < \alpha < 57^\circ$) is found to give the highest performance.

Effects of payloads. In the above studies, the mass, M, and damping coefficient, c, in the payload were fixed. Here we investigate the effects of these two parameters on the performance of the DCDEA. L is fixed at 21 mm and λ_p is 1×1. **Figure 5** (**b**) shows the peak power output, the corresponding frequency and the peak stroke against M. As M increases, P_{peak} and Δd_{peak} also rise while the frequency decreases and when M is heavier than 10 g, P_{peak} also reduces. Increasing damping in the payload significantly decreases P_{peak}, Δd_{peak} and f_{peak}, as plotted in **Figure 5** (**c**). The sharp reduction in power output is believed to be due to the force generated by the DCDEA which cannot overcome the velocity-proportional damping force when the damping coefficient is large, which results in greatly reduced actuation amplitude thus low power output. In applications where high damping exists, multiple layers of membranes can be stacked to achieve the desired power output.

By using the dynamic model developed in this work, the optimal working frequency range of the DCDEA under different payload conditions can be found. **Figure 6** (**a**) shows examples of the power output of the DCDEA against frequency for three different mass values. The optimal working frequency range for each case is also highlighted in **Figure 6** (**a**), which is defined as the frequency range where the power output is greater than 80% of its peak value.

Effects of charging/discharging rate. The surface resistance of a DCDEA directly affects its charging and discharging rate (characterized using a RC constant, where R is the resistance and C is the capacitance), which is determined by the compliant electrode material used in fabrication. An order of magnitude study is conducted here to investigate the effects of RC constant (via varying the surface resistance from 0.1 to 10 MΩ by orders of magnitude, while fixing the capacitance value at 0.4 nF, as measured in the experiments) on the power output of the DCDEA and the results are shown in **Figure 6** (**b**). A dramatic increase in the power output can be found when the RC constant is reduced by one order of magnitude, which demonstrates the significance of developing compliant electrode materials with improved conductivity [40].

In this section, the effects of the physical parameters of the actuator, the mechanical and electrical (RC constant) payloads on the power output were investigated. In practical applications, once these parameters and payload conditions are known, the optimal operational frequency range can be determined using this model. Vice versa, if the mechanical payload and the target working frequency range are given, this model can be used as a guideline for determining the DCDEA design parameters (λ_p, L, layer numbers). Note that the power optimization study setup adopted in this work can also be used for the optimization of other DEA configurations and various dissipative payload cases. For example, nonlinear viscous damping (aerodynamic load) or Coulomb damping (friction) in real systems can be replaced by the linear viscous damping by ensuring the same energy dissipation per cycle to enable the use of this setup.

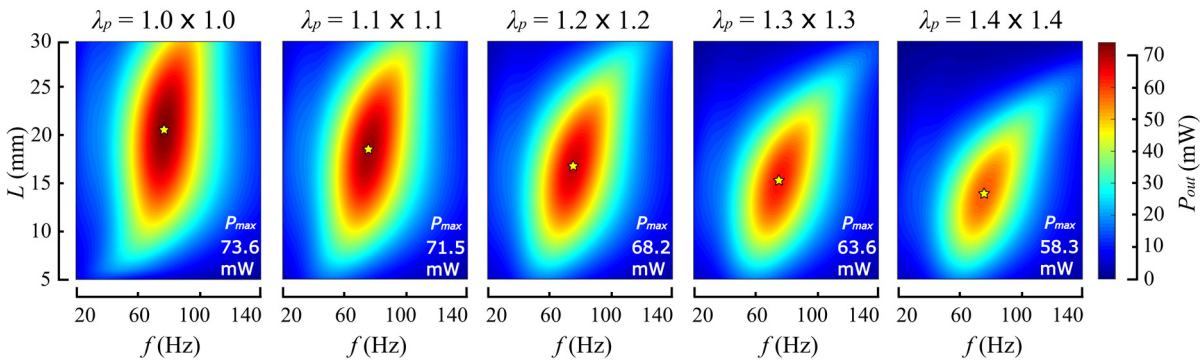

Figure 4. Effects of pre-stretch ratio and spacer length on power output of the DCDEA. Yellow stars mark the maximum P_{out} value for each λ_p. (c = 1 N.s/m, M = 1 g).

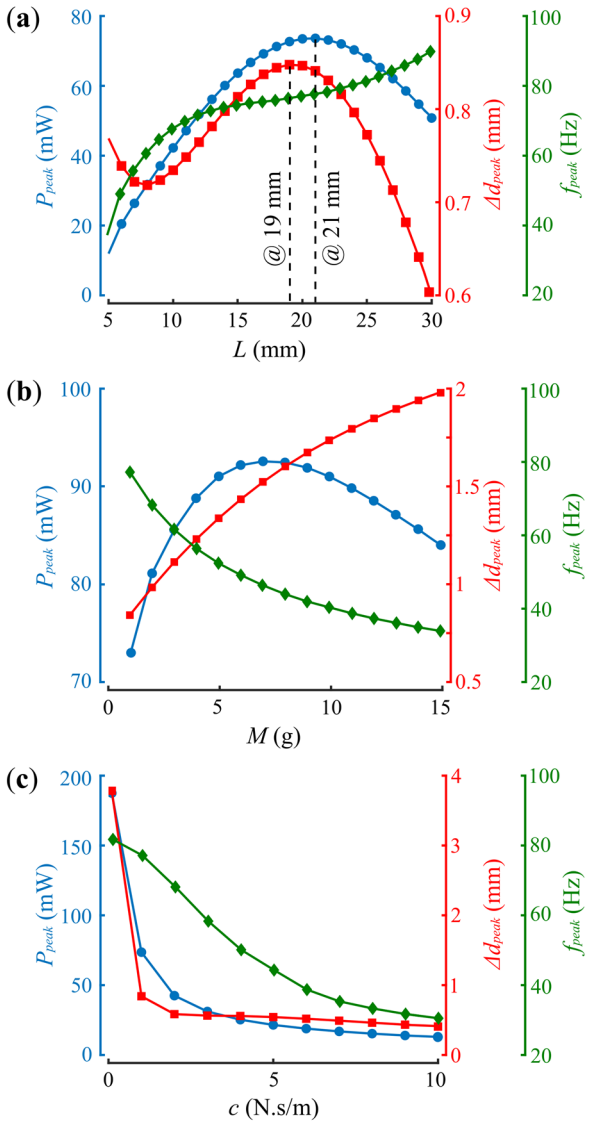

Figure 5. Detailed parametric study on the power output of the DCDEA. (**a**) Effects of spacer length on P_{peak}, Δd_{peak} and f_{peak} (λ_p = 1× 1, c = 1 N.s/m, M = 1 g). (**b**) Effects of mass on P_{peak}, Δd_{peak} and f_{peak} (λ_p

= 1×1, L = 21 mm, c = 1 N.s/m). (**c**) Effects of damping coefficient on P_{peak}, Δd_{peak} and f_{peak} (λ_p = 1×1, L = 21 mm, M = 1 g). (color figure in print)

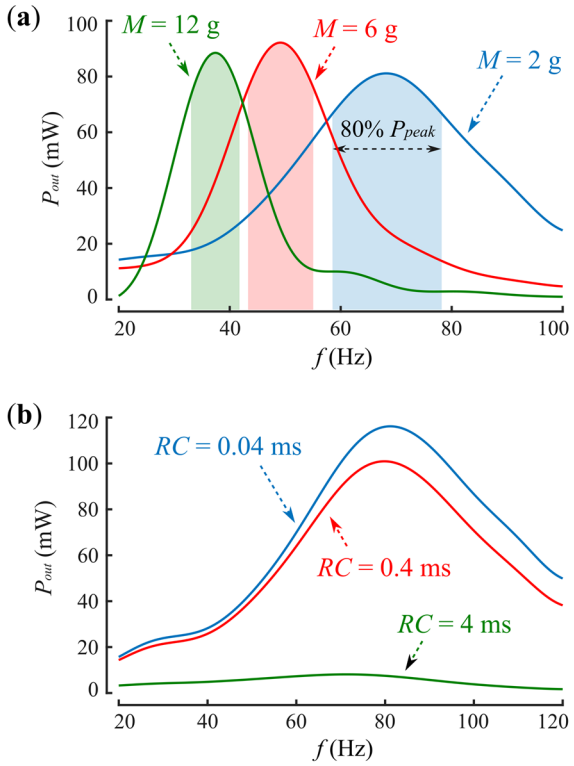

Figure 6. (**a**) Examples of determining the optimal working frequency range with different payload conditions. (λ_p = 1×1, L = 21 mm, c = 1 N.s/m) (**b**) Examples of the effects of RC time constant on the power output of DCDEAs. (λ_p = 1×1, L = 21 mm, c = 1 N.s/m, M = 1 g, the surface resistance, R_s is varied while keeping capacitance, C, constant) (color figure in print)

5. DCDEA driven flapping wing mechanism design

5.1 Design overview

To demonstrate the resonant actuation principle of DCDEAs, in this section we present a DCDEA driven flapping wing mechanism (FWM), as illustrated in **Figure 7** (**a**). FWMs for untethered robotic flight have demanding mass-specific power density requirements, which make them well suited for demonstrating the benefits of resonant power optimization. A DCDEA stack with the optimal parameters determined in Section 4 (a = 7.5 mm, b = 15 mm, L = 21 mm, λ_p = 1× 1) drives the wings via a rack and pinion mechanism. A fabricated prototype of the FWM is shown in **Figure 7** (**b**). The main structure was fabricated via 3D printing (Eden 350V printer, Objet Geometries). Rack and pinions have a pitch of 0.5 MOD and the pinions are precision spur gears with the pitch circle diameter of 6

mm (Accu, UK). The wings are 50 mm in length and 20 mm in width and are made of 0.05 mm thickness Mylar (DuPont).

5.2 Performance characterization

Figure 7 (**c**) shows the measured flapping stroke against actuation frequency for DCDEAs with 1, 2, and 4 membrane layers. Distinguishable stroke peaks can be observed for all three cases, showing clear resonance of the system. As the number of layers increases, both the peak flapping stroke and its corresponding frequency increases. For the 4-layer one, the FWM has a highest flapping stroke of 31˚ at 30.2 Hz. As the number of layers increases further, saturation is caused by the high voltage amplifier used in this work which is not capable of driving the increasing electrical payload. As a result, a maximum of 4 layers were used in the experiment. The detailed actuation voltages and the displacement of DCDEA with 4-layer stack are shown in **Figure 7** (**d**), where the blue and red colours represent the up and downstroke of the wings. It can be noted that due to the electrical payload, the programmed square waves turned trapezoidal, which demonstrates the demand for a high-power amplifier in order to maximize the power output of the DEAs.

The flapping motion of the FWMAV at 30 Hz was recorded using a high-speed camera and **Figure 7** (**e**) shows a series of footages in one cycle. It can be noted that the wings pitch passively during the up and downstrokes due to the aerodynamic load and, during the stroke reversal, the wings' pitch reverses passively to change the direction of angle-of-attack due to the inertia of the wings and the added mass of the air [41]. Such passive wing pitch reversal has been observed in insect flight [42].

5.3 Discussion

The FWM design proposed in this work serves as a demonstrator of the resonant actuation of DCDEAs. The resonant peaks observed in the FWM proves the feasibility of utilizing the inherent elasticity in DEAs to achieve a resonant flapping motion, as found in natural counterparts, which maximizes the power output and energy efficiency of the actuators. Improvements can be made to increase the mass-specific power density by using electrodes with better conductivity [45] and reducing the mass of the support frame [1]. Developing miniature yet high-power high voltage amplifiers is also an essential aspect for enabling untethered DEA driven FWMAVs. Nonetheless, the improved power output from a resonating DCDEA demonstrated by this FWM shows the promise for resonating DEAs to be exploited for other forms of dynamic robotic locomotion and applications such as active vibrational damping.

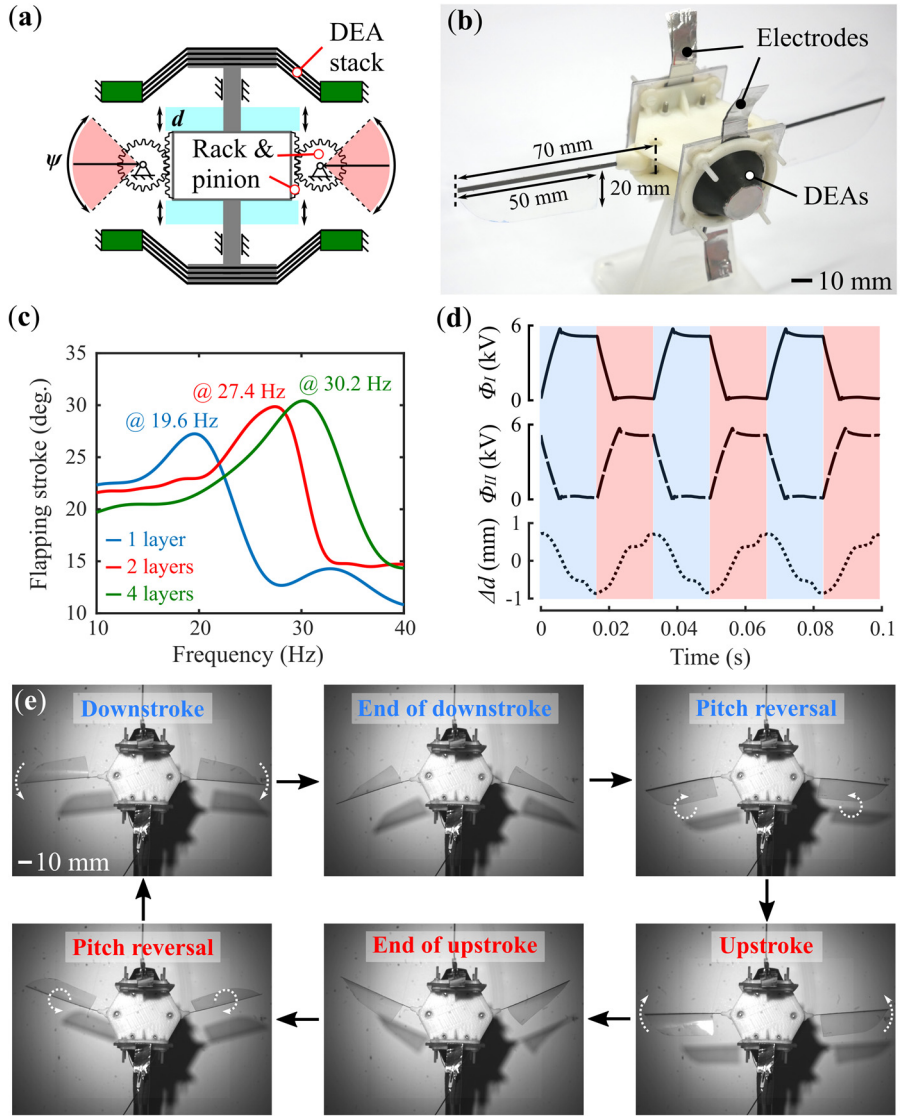

Figure 7. DCDEA driven flapping wing prototype. (**a**) Schematic diagram of DCDEA driven FWM design. (**b**) Photo of fabricated FWM prototype. (**c**) Flapping stroke against excitation frequency of DCDEA with different layers. (**d**) Example of actuation voltages and DEA displacement at 30.2 Hz. (**e**) Series of flapping motion in one cycle. (multimedia file available in supplementary material) (color figure in print)

6. Conclusion

The inherent elasticity of DEAs offers a clear advantage in achieving resonant actuations over conventional actuators as no additional elastic elements are required. In this work, a DCDEA configuration was adopted and a maximum resonant stroke of 257 % relative to its height was measured. A numerical model was developed to characterize its dynamic response. With this model, the power output of DCDEA was optimized against its pre-stretch ratio and spacer length. Optimization results showed that the design with no pre-stretch and a spacer length to membrane radius of 1.4 results in the

highest power output with the power density comparable to insect muscles. A bioinspired flapping wing mechanism was developed to demonstrate the resonant actuation of the DCDEA and a peak flapping stroke of 31˚ at 30 Hz was recorded. The power optimization framework developed in this work is believed to be useful in power characterization and optimization of various configurations of DEAs under different dissipative payloads. The high resonant amplitude and power output of the DCDEAs can also benefit other dynamic applications in vibrational control, soft motors and energy harvesting.

Acknowledgement

C. Cao appreciates the support from the EPSRC Centre for Doctoral Training in Future Autonomous and Robotic Systems (FARSCOPE) at the Bristol Robotics Laboratory. A. Conn and X. Gao acknowledge support from EPSRC grant EP/P025846/1.

References

[1] K. Ma, P. Chirarattananon, S. B. Fuller, and R. J. Wood, "Controlled Flight of a Biologically Inspired, Insect-Scale Robot," *Science (80-.).*, vol. 340, no. 6132, pp. 603–607, 2013.

[2] M. Karasek, F. T. Muijres, C. De Wagter, B. D. W. Remes, and G. C. H. E. De Croon, "A tailless aerial robotic flapper reveals that flies use torque coupling in rapid banked turns," *Science (80-.).*, vol. 361, no. 6407, pp. 1089–1094, 2018.

[3] M. H. Dickinson and M. S. Tu, "The function of dipteran flight muscle," *Comp. Biochem. Physiol. - A Physiol.*, vol. 116, no. 3, pp. 223–238, 1997.

[4] C. P. Ellington, "The novel aerodynamics of insect flight: applications to micro-air vehicles," *J. Exp. Biol.*, vol. 202, no. 23, pp. 3439–3448, 1999.

[5] R. Pelrine, R. Kornbluh, Q. Pei, and J. Joseph, "High-speed electrically actuated elastomers with strain greater than 100%," *Science (80-.).*, vol. 287, no. 5454, pp. 836–839, 2000.

[6] S. Rosset and H. R. Shea, "Small, fast, and tough: Shrinking down integrated elastomer transducers," *Appl. Phys. Rev.*, vol. 3, no. 3, p. 031105, 2016.

[7] J. W. Fox and N. C. Goulbourne, "Electric field-induced surface transformations and experimental dynamic characteristics of dielectric elastomer membranes," *J. Mech. Phys. Solids*, vol. 57, no. 8, pp. 1417–1435, 2009.

[8] J. Zhu, S. Cai, and Z. Suo, "Resonant behavior of a membrane of a dielectric elastomer," *Int. J. Solids Struct.*, vol. 47, no. 24, pp. 3254–3262, 2010.

[9] J. Zhao, J. Niu, D. McCoul, Z. Ren, and Q. Pei, “Phenomena of nonlinear oscillation and special resonance of a dielectric elastomer minimum energy structure rotary joint,” *Appl. Phys. Lett.*, vol. 106, no. 13, p. 133504, 2015.

[10] P. Rothemund, X. P. Morelle, K. Jia, G. M. Whitesides, and Z. Suo, “A Transparent Membrane for Active Noise Cancelation,” *Adv. Funct. Mater.*, vol. 28, no. 29, pp. 1–8, 2018.

[11] C. Tang, B. Li, W. Sun, Z. Li, and H. Chen, “Identification and characterization of the out-of-plane resonance in a dielectric elastomer to drive an agile robotic cube,” *J. Appl. Phys.*, vol. 122, no. 16, p. 165104, 2017.

[12] Z. Lu, H. Godaba, Y. Cui, C. C. Foo, M. Debiasi, and J. Zhu, “An electronically tunable duct silencer using dielectric elastomer actuators,” *J. Acoust. Soc. Am.*, vol. 138, no. 3, pp. EL236–EL241, 2015.

[13] U. Gupta, H. Godaba, Z. Zhao, C. K. Chui, and J. Zhu, “Tunable force/displacement of a vibration shaker driven by a dielectric elastomer actuator,” *Extrem. Mech. Lett.*, vol. 2, no. 1, pp. 72–77, 2015.

[14] B. Li, J. Zhang, L. Liu, H. Chen, S. Jia, and D. Li, “Modeling of dielectric elastomer as electromechanical resonator,” *J. Appl. Phys.*, vol. 116, no. 12, p. 124509, 2014.

[15] B. Li, J. Zhang, H. Chen, and D. Li, “Voltage-induced pinnacle response in the dynamics of dielectric elastomers,” *Phys. Rev. E*, vol. 93, no. 5, p. 052506, 2016.

[16] C. Tang, B. Li, H. Fang, Z. Li, and H. Chen, “A speedy, amphibian, robotic cube: Resonance actuation by a dielectric elastomer,” *Sensors Actuators, A Phys.*, vol. 270, pp. 1–7, 2018.

[17] C. Cao, R. S. Diteesawat, J. Rossiter, and A. T. Conn, “A Reconfigurable Crawling Robot Driven by Electroactive Artificial Muscle,” in *IEEE International Conference on Soft Robotics (RoboSoft) 2019*, 2019, pp. 840–845.

[18] X. Gao, C. Cao, J. Guo, and A. T. Conn, “Elastic Electroadhesion with Rapid Release by Integrated Resonant Vibration,” *Adv. Mater. Technol.*, vol. 4, no. 1, p. 1800378, 2019.

[19] C. Cao, X. Gao, and A. T. Conn, “A compliantly coupled dielectric elastomer actuator using magnetic repulsion,” *Appl. Phys. Lett.*, vol. 114, no. 1, p. 011904, 2019.

[20] C. Cao, X. Gao, and A. T. Conn, “A Magnetically Coupled Dielectric Elastomer Pump for Soft Robotics,” *Adv. Mater. Technol.*, vol. 4, no. 8, p. 1900128, 2019.

[21] Y. Chen *et al.*, “Controlled flight of a microrobot powered by soft artificial muscles,” *Nature*, vol. 575, 2019.

[22] A. T. Conn and J. Rossiter, “Towards holonomic electro-elastomer actuators with six degrees of freedom,” *Smart Mater. Struct.*, vol. 21, no. 3, p. 035012, 2012.

[23] M. Follador, M. Cianchetti, and B. Mazzolai, “Design of a compact bistable mechanism based on dielectric elastomer actuators,” *Meccanica*, vol. 50, no. 11, pp. 2741–2749, 2015.

[24] F Branz and A Francesconi, “Modelling and control of double cone dielectric elastomer actuator,” *Smart Mater. Struct.*, vol. 25, no. 9, p. 095040, 2016.

[25] C. Cao, T. L. Hill, and A. T. Conn, “On the nonlinear dynamics of a circular dielectric elastomer oscillator,” *Smart Mater. Struct.*, vol. 28, no. 7, p. 075020, 2019.

[26] C. Cao, X. Gao, and A. T. Conn, “Towards efficient elastic actuation in bio-inspired robotics using dielectric elastomer artificial muscles,” *Smart Mater. Struct.*, vol. 28, no. 9, p. 095015, 2019.

[27] C. Cao, T. L. Hill, A. T. Conn, B. Li, and X. Gao, “Nonlinear Dynamics of a Magnetically Coupled Dielectric Elastomer Actuator,” *Phys. Rev. Appl.*, vol. 12, no. 4, p. 044033, 2019.

[28] M. Hodgins, G. Rizzello, D. Naso, A. York, and S. Seelecke, “An electro-mechanically coupled model for the dynamic behavior of a dielectric electro-active polymer actuator,” *Smart Mater. Struct.*, vol. 23, no. 10, p. 104006, 2014.

[29] G. Rizzello, M. Hodgins, D. Naso, A. York, and S. Seelecke, “Modeling of the effects of the electrical dynamics on the electromechanical response of a DEAP circular actuator with a mass-spring load,” *Smart Mater. Struct.*, vol. 24, no. 9, p. 094003, 2015.

[30] X. Li, W. Li, W. Zhang, H. Zou, Z. Peng, and G. Meng, “Magnetic force induced tristability for dielectric elastomer actuators,” *Smart Mater. Struct.*, vol. 26, no. 10, p. 105007, 2017.

[31] G. Berselli, R. Vertechy, G. Vassura, and V. Parenti-Castelli, “Optimal synthesis of conically shaped dielectric elastomer linear actuators: Design methodology and experimental validation,” *IEEE/ASME Trans. Mechatronics*, vol. 16, no. 1, pp. 67–79, 2011.

[32] A. . Gent, “A New Constitutive Relation for Rubber,” *Rubber Chem. Technol.*, vol. 69, no. 1, pp. 59–61, 1996.

[33] C. Chiang Foo, S. Cai, S. Jin Adrian Koh, S. Bauer, and Z. Suo, “Model of dissipative dielectric elastomers,” *J. Appl. Phys.*, vol. 111, no. 3, p. 034102, 2012.

[34] D. Gatti, H. Haus, M. Matysek, B. Frohnapfel, C. Tropea, and H. F. Schlaak, “The dielectric breakdown limit of silicone dielectric elastomer actuators,” *Appl. Phys. Lett.*, vol. 104, no. 5, p. 052905, 2014.

[35] S. Zakaria, P. H. F. Morshuis, M. Y. Benslimane, L. Yu, and A. L. Skov, “The electrical breakdown strength of pre-stretched elastomers, with and without sample volume conservation,” *Smart Mater. Struct.*, vol. 24, no. 5, p. 055009, 2015.

[36] F. Forster-Zugel, S. Solano-Arana, F. Hlug, and H. Schlaak, “Dielectric breakdown strength measurements with silicone-based single-layer dielectric elastomer transducers,” *Smart Mater. Struct.*, 2019.

[37] C. Cao and A. T. Conn, “Performance Optimization of a Conical Dielectric Elastomer Actuator,” *Actuators*, vol. 7, no. 2, p. 32, 2018.

[38] R. D. Stevenson and R. K. Josephson, “Effects of operating frequency and temperature on mechanical power output from moth flight muscle,” *J. Exp. Biol.*, vol. 149, no. 1, pp. 61–78, 1990.

[39] P. Chai and D. Millard, “Flight and size constraints: hovering performance of large hummingbirds under maximal loading.,” *J. Exp. Biol.*, vol. 200, no. 21, pp. 2757–2763, 1997.

[40] H. Zhao, A. M. Hussain, M. Duduta, D. M. Vogt, R. J. Wood, and D. R. Clarke, “Compact Dielectric Elastomer Linear Actuators,” *Adv. Funct. Mater.*, vol. 28, no. 42, p. 1804328, 2018.

[41] S. P. Sane, “The aerodynamics of insect flight,” *J. Exp. Biol.*, vol. 206, no. 23, pp. 4191–4208, 2003.

[42] A. J. Bergou, S. Xu, and Z. J. Wang, “Passive wing pitch reversal in insect flight,” *J. Fluid Mech.*, vol. 591, pp. 321–337, 2007.

[43] G. K. Lau, H. T. Lim, J. Y. Teo, and Y. W. Chin, “Lightweight mechanical amplifiers for rolled dielectric elastomer actuators and their integration with bio-inspired wing flappers,” *Smart Mater. Struct.*, vol. 23, no. 2, p. 025021, 2014.

[44] E.-F. M. Henke, K. E. Wilson, and I. A. Anderson, “Entirely soft dielectric elastomer robots,” in *Electroactive Polymer Actuators and Devices (EAPAD) 2017*, 2017, vol. 10163, p. 101631N.

[45] M. Duduta, E. Hajiesmaili, H. Zhao, R. J. Wood, and D. R. Clarke, “Realizing the potential of dielectric elastomer artificial muscles,” *Proc. Natl. Acad. Sci.*, vol. 116, no. 7, pp. 2476–2481, 2019.

[46] T. Van Truong, U. Kureemun, V. B. C. Tan, and H. P. Lee, “Study on the structural optimization of a flapping wing micro air vehicle,” *Struct. Multidiscip. Optim.*, vol. 57, no. 2, pp. 653–664, 2017.

[47] L. Zhao, Q. Huang, X. Deng, and S. P. Sane, “Aerodynamic effects of flexibility in flapping wings,” *J. R. Soc. Interface*, vol. 7, no. 44, pp. 485–497, 2010.

Supplementary material

DCDEA fabrication

To fabricate the DCDEA, an off-the-shelf silicone elastomer (ELASTOSIL, thickness 100 μm, Wacker Chemie AG) was used as the membrane. The membrane was first pre-stretched biaxially by a ratio of λ_p, and then bonded to an acrylic ring (15 mm inner radius) by silicone transfer tape (ARclear 93495, Adhesives Research). A disk magnet (7.5 mm outer radius) was bonded to the centre of the membrane using the same method. Copper tapes were used as the connection between the custom-made carbon electrodes and high voltage cables. The rod was fabricated by having two disk magnets bonded to a Nylon spacer. The two magnets were ensured an attraction coupling with the disk magnets attached to the membranes. The DCDEA was assembled by having the rod attracted to the two DEA membranes and then fixed by fasteners.

Carbon electrode fabrication

The fabrication process of the custom carbon grease is described as follows. First, 10/15/20 wt.% carbon black powders (1333-86-4, Cabot Corporation, USA) and 80 wt.% vegetable (rapeseed) oil (ASDA, UK) were added to a mixing cup. The mixture was first stirred by a mixer (Model 50006-13, Cole-Parmer, UK) at the speed of 100 rpm for 1 min and then 600 rpm for 5 mins to achieve a homogenous dispersion. The custom carbon grease is found to be compatible with the ELASTOSIL silicone material, as reported in our previous work.

Quasi-static force-displacement test setup

To measure its quasi-static force-displacement relationship, a single cone DEA frame was fixed to the testing rig and a linear rail (X-LSQ150B-E01, ZABER) deformed the centre of the DEO membrane out-of-plane at a low velocity of 0.05 mm/s to ensure negligible viscoelasticity. A constant voltage was generated by a high voltage amplifier (5HV23-BP1, Ultravolt) and was applied to the dEA during deformation to analyse the effect of electric field on the force-displacement relationship. The voltage amplitude was determined by $\Phi = E\lambda_p^2/H_0$, where E = 50 V/μm. A load cell (NO.1004, TEDEA) was used to measure the reaction force of the DEO and a laser displacement sensor (LK-G152 and LKGD500, Keyence) was used to measure the deformation of the DEO membrane. All signals were collected by a DAQ device (National Instruments, BNC-2111) at a sampling frequency of 10,000 Hz and controlled by MATLAB (MathWorks).

Dynamic response test setup

A frequency step test was performed to investigate the dynamic response of the DEA. The same laser displacement sensor and DAQ device from quasi-static test setup were used here. The DCDEA frame was fixed to the testing rig, while leaving the central rod to move freely. two varying-frequency sinusoidal voltage signals were generated by MATLAB and applied to the DCDEA via a high voltage amplifier. A laser displacement sensor measured the out-of-plane deformation of the rod of the DCDEA at a sampling frequency of 40,000 Hz. The excitation frequency was stepped forward from 1 to 100 Hz at the step of 0.05 Hz. The voltage amplitude was determined by by $\Phi = E\lambda_p^2/H_0$, where E = 50 V/μm.